Spontaneous Parametric Down-Conversion in 4H-SiC Integrated Platform

*Xiaodong Shi, Angela Anna Baiju, Veerendra Dhyani, Sihao Wang, Sakthi Sanjeev Mohanraj, Victor Leong, Jiapeng Sun, Boyang Deng, Jingjing Zhang, Yongsheng Wang, Karsten Rottwitt, Haiyan Ou, and Di Zhu**

4H-silicon carbide (SiC) has recently emerged as a promising material for nonlinear photonic integrated circuits, thanks to its low loss, wide bandgap, as well as strong second-order ($\chi^{(2)}$) and third-order ($\chi^{(3)}$) nonlinearities. Though its unique crystal structure allows versatile $\chi^{(2)}$ processes, spontaneous parametric down-conversion (SPDC) still remains unrealized. In this work, photon-pair generation in a 4H-SiC-on-insulator integrated platform is demonstrated through modal-phase-matched type-I SPDC. Furthermore, type-0 and type-II $\chi^{(2)}$ nonlinear interactions are shown in 4H-SiC waveguides, thus highlighting the potential to exploit diverse phase-matching mechanisms on this platform. These results underscore the potential of 4H-SiC for advancing the development of integrated quantum photonics in the realms of quantum information processing and quantum communication.

1. Introduction

Silicon carbide (SiC) is a technologically important material for both microelectronics and optoelectronics.[1,2] Its exceptional thermal conductivity, wide bandgap, high breakdown voltage, and robust mechanical and chemical properties have made it ideal for high-power, high-frequency, high-radiation, and high-temperature applications. In the past decade, it has also attracted significant interest in integrated photonics, thanks to its broad transparent window from near ultraviolet to mid-infrared, high refractive index, strong electro-optic effect, and high optical nonlinearities.[3–5] Its fabrication process is also fully compatible with the complementary metal-oxide semiconductor (CMOS) technology.[6] Among various polytypes, 4H-, 3C-, and amorphous SiC are the most popular for nonlinear optical applications.[7–19] Amorphous SiC shows strong third-order nonlinearity ($\chi^{(3)}$) but no material-based second-order nonlinearity ($\chi^{(2)}$) due to the lack of noncentrosymmetry. 4H- and 3C-SiC exhibit both $\chi^{(2)}$ and $\chi^{(3)}$ nonlinearities, enabling efficient wavelength conversion and electro-optic modulation. Compared to 3C-SiC, 4H-SiC has lower optical loss, broader transparent window towards short wavelengths, higher refractive index, diverse nonlinear coefficients, and higher thermo-optic coefficient, making it a promising platform for multifunctional and nonlinear integrated photonics.[20–22]

Quantum light sources are important building blocks for photonic quantum technologies, from quantum communication and networks to computing and sensing.[23–26] SiC allows mono-

X. Shi, A. A. Baiju, V. Dhyani, S. Wang, S. S. Mohanraj, D. Zhu
A*STAR Quantum Innovation Centre (Q.InC), Agency for Science, Technology and Research (A*STAR)
Singapore 138634, Singapore
E-mail: dizhu@nus.edu.sg

X. Shi, A. A. Baiju, V. Dhyani, S. Wang, S. S. Mohanraj, V. Leong, D. Zhu
Institute of Materials Research and Engineering (IMRE), Agency for Science, Technology and Research (A*STAR)
Singapore 138634, Singapore

The ORCID identification number(s) for the author(s) of this article can be found under https://doi.org/10.1002/lpor.202500104

DOI: 10.1002/lpor.202500104

X. Shi, Y. Wang, K. Rottwitt, H. Ou
Department of Electrical and Photonics Engineering
Technical University of Denmark
Kgs. Lyngby 2800, Denmark

A. A. Baiju
Department of Physics
National University of Singapore
Singapore 117542, Singapore

J. Sun, D. Zhu
Department of Materials Science and Engineering
National University of Singapore
Singapore 117575, Singapore

B. Deng, D. Zhu
Centre for Quantum Technologies
National University of Singapore
Singapore 117543, Singapore

J. Zhang
Institute of Mirco/Nano Optoelectronic and Terahertz Technology
Jiang Su University
Zhenjiang 210010, China

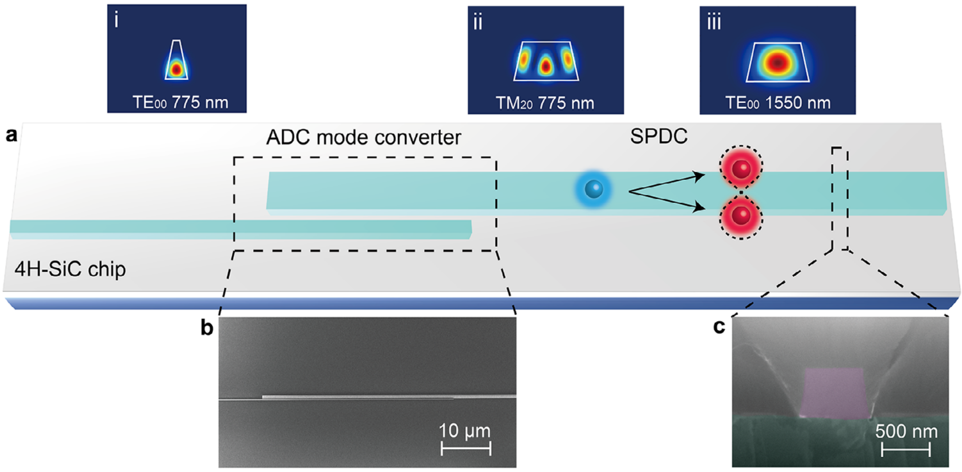

Figure 1. Spontaneous parametric down-conversion in 4H-SiCOI integrated photonic platform. a) Schematic of the 4H-SiC waveguides for producing telecom photon pairs through SPDC, which consists of a narrow waveguide supporting TE_{00} mode at 775 nm, an asymmetric-directional-coupler based mode converter to convert the TE_{00} mode to a TM_{20} mode at 775 nm, and a wide waveguide for modal phase matching with the TE_{00} mode at 1550 nm. Mode profiles ($|E|^2$) of (i) TE_{00} mode at 775 nm in the narrow waveguide, (ii) TM_{20} mode at 775 nm, and (iii) TE_{00} mode at 1550 nm in the wide waveguide. b) A top-view SEM image of the mode converter. c) A false-colored cross-section SEM image of the SiC waveguide for SPDC.

lithic integration of quantum light sources, either in the form of defect centers or through nonlinear processes.[27,28] In 4H-SiC, various optically addressable spin defects have been demonstrated across the visible to near-infrared wavelength range, such as silicon vacancy, divacancy, carbon antisite vacancy, D_1 center, nitrogen vacancy, and transition metal impurity related color centers, which can be used as deterministic single-photon sources.[29–35] A heralded single-photon source at telecom wavelengths based on photon-pair generation through spontaneous four-wave mixing has been recently demonstrated using 4H-SiC microring resonators ($\chi^{(3)}$ nonlinearity).[36] In fact, 4H-SiC is also known for its strong $\chi^{(2)}$ nonlinearity.[37] Second-harmonic generation in its nanophotonic waveguides and microring resonators has been observed.[38,39] These also make possible the production of photon pairs via spontaneous parametric down-conversion (SPDC). To date, however, SPDC in 4H-SiC waveguides has not been demonstrated. SPDC based quantum light sources in $\chi^{(2)}$ optical materials can usually benefit from high pair-generation efficiency, large wavelength separation between the pump and the single photons for easy pump filtering, as well as the potential of integration with fast electro-optic modulators.[40,41]

In this work, we experimentally demonstrate second-harmonic generation (SHG) and SPDC photon-pair generation in the 4H-SiC-on-insulator (4H-SiCOI) integrated platform. By engineering the waveguide dimension, we realize type-I modal phase matching (MPM), achieving normalized SHG efficiency of 12.6 ± 0.2%$\mathrm{W}^{-1}\mathrm{cm}^{-2}$ and telecom photon-pair generation with a rate of 3.4×10^4 Hz mW^{-1} (within a 15 nm filtered bandwidth). With systematic studies on the polarization-dependent phase-matching functions, we also observe type-0 and type-II nonlinear processes in the waveguides. Our work showcases the potential for flexible and versatile classical and quantum $\chi^{(2)}$ wavelength conversion in the 4H-SiC photonic integrated platform.

2. Results

The schematic for SPDC photon-pair generation in a 500 nm thick 4H-SiC photonic integrated circuit is depicted in **Figure 1a**. This nonlinear process relies on modal phase matching between the TM_{20} mode at 775 nm (pump) and the TE_{00} mode at 1550 nm (signal and idler). To efficiently excite the 775 nm TM_{20} mode in the waveguide, an asymmetric directional coupler (ADC) mode converter is used. The mode converter consists of a narrow waveguide (135 nm width) designed to support the 775 nm TE_{00} mode, and a wide waveguide (600 nm width) optimized to support the TM_{20} mode. With a gap of 220 nm and a length of 40 µm, the converter achieves a conversion efficiency of approximately 80%, effectively transforming the TE_{00} mode into the TM_{20} mode and further facilitating the modal-phase-matched SPDC process.

4H-SiC belongs to the 6mm symmetry group. The hexagonal crystal space-group symmetry results in five nonvanishing elements in its $\chi^{(2)}$ nonlinear susceptibility tensor, including d_{15}, d_{24}, d_{31}, d_{32}, and d_{33}. Here, we investigate the type-I phase matching utilizing d_{31} in c-cut 4H-SiC nanophotonic waveguides, where the generated field has a different polarization from the incident field. The type-I SHG phase-matching wavelength between the fundamental-harmonic (FH) transverse-electric (TE) wave and the second-harmonic (SH) transverse-magnetic (TM) wave is controlled by tailoring the waveguide geometry. Based on MPM, we find that a width of ≈600 nm allows the effective index of the TE_{00} mode at 1550 nm to match that of the TM_{20} mode at 775 nm (**Figure 2a**), in a 500 nm thick 4H-SiC waveguide with a sidewall angle of 80°. When the phase-matching condition is fulfilled, the normalized SHG conversion efficiency follows $\eta = \frac{P_{SH}}{P_{FH}^2 L^2} = \frac{8\pi^2}{\epsilon_0 c n_{eff}^3 \lambda^2} d_{eff}^2 \Gamma$, where P_{SH} is the generated SH power, P_{FH} is the pump power of the FH wave, L is the length of the phase-matched waveguide, ϵ_0 is the free-space permittivity, c is the speed of light, λ is the FH wavelength, n_{eff} is the effective index, and d_{eff} is the effective second-order nonlinear coefficient (d_{eff} =

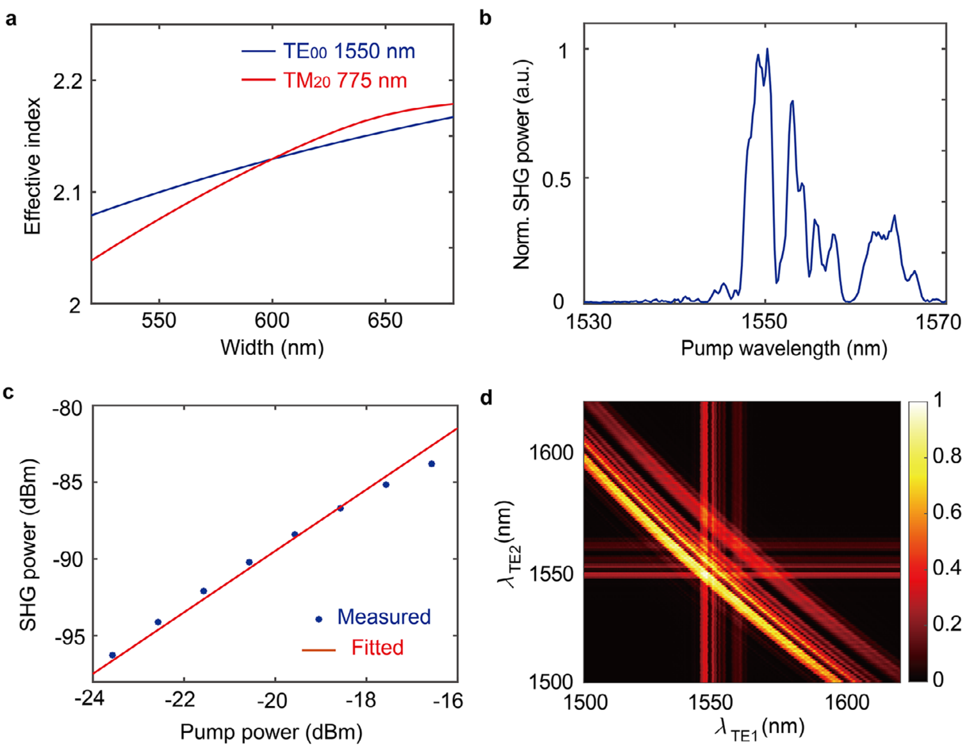

Figure 2. Type-I phase-matched $\chi^{(2)}$ nonlinear wavelength conversion in 4H-SiC nanophotonic waveguides. a) Simulation of effective indices of the TE_{00} mode at 1550 nm (blue) and TM_{20} mode at 775 nm (red) as a function of the SiC waveguide width. The intersection point at 600 nm between the blue and red curves corresponds to the phase-matching point for MPM. b) Measured SHG power as a function of pump wavelength. c) Measured SHG power as a function of on-chip pump power in a 3 mm long 4H-SiC waveguide. A linear fitting reveals an on-chip conversion efficiency of 12.6 ± 0.2% $W^{-1}cm^{-2}$. d) Measured SFG phase-matching function from 1480 to 1630 nm, allowing broadband three-wave mixing processes. The colorbar shows the normalized visible photon counts from SFG.

$d_{31} = 6.5$ pm V^{-1}).[42]. It is noted that the second-order nonlinear coefficient of 4H-SiC may have slight variations depending on the crystal quality or doping concentrations.[43,44] Γ is the nonlinear coupling parameter between the FH and SH modes, given by $\Gamma = \frac{|\int_{\mathrm{SiC}} (E^*_{x,\mathrm{FH}})^2 E_{z,\mathrm{SH}} \mathrm{d}x\mathrm{d}z|^2}{|\int_{\mathrm{all}} |E_{\mathrm{FH}}|^2 \mathrm{d}x\mathrm{d}z|^2 \int_{\mathrm{all}} |E_{\mathrm{SH}}|^2 \mathrm{d}x\mathrm{d}z}$, where E is the corresponding electric field.[45] We theoretically calculate the normalized type-I SHG conversion efficiency in this 4H-SiC nanophotonic waveguide to be $\eta_{\mathrm{sim}} = 68\ \%\ \mathrm{W}^{-1}\mathrm{cm}^{-2}$, where $\Gamma = 0.11\ \mu\mathrm{m}^{-2}$ here.

The fabrication of 4H-SiC waveguides is carried out on a c-cut 500 nm thick 4H-SiCOI chip. The waveguides are patterned using electron-beam (e-beam) lithography followed by inductively coupled plasma reactive ion etching (ICP-RIE) with hydrogen silsesquioxane (HSQ) e-beam resist as the etch mask. Silicon dioxide cladding is deposited using ICP chemical vapor deposition (ICP-CVD) to cover the waveguides. A scanning electron micrograph (SEM) of the waveguide cross section is shown in Figure 1c.

We first characterize the nonlinear efficiency and phase matching functions through SHG and sum-frequency generation (SFG). These measurements are performed in a 3 mm long single straight waveguide. A telecom continuous-wave (CW) tunable laser is aligned to the TE polarization and coupled to the waveguide through a lensed fiber. The generated SH signal at the output is collected using an aspheric lens, filtered by a short-pass filter, and sent to a silicon avalanche photodiode (APD). The APD is synchronized with the laser sweep, ensuring that the detected photons corresponded to the respective SH wavelengths. The measured SHG spectrum is shown in Figure 2b. By converting the APD count rate to power and taking into account the coupling and detection efficiencies, we get the on-chip SHG power at the peak SHG wavelength as a function of the pump power (Figure 2c). A linear fitting slope of two in the log-log plot confirms the quadratic relation between SH and FH powers. We fit the measurement results and get a normalized on-chip SHG conversion efficiency of $\eta_{\mathrm{exp}} = 12.6 \pm 0.2\%\ \mathrm{W}^{-1}\mathrm{cm}^{-2}$. This efficiency is lower than the theoretical prediction, mainly due to the geometry fluctuation, e.g., thickness variation, which shifts the optimal phase-matching wavelength along the waveguide, as seen in the measured SHG spectral response (Figure 2b). We further measure SFG using two independent telecom CW lasers, which are combined using a 50/50 beam splitter and coupled into the waveguide. By tuning the pump wavelengths and monitoring the APD count rate, we map out the type-I phase-matching function (Figure 2d), indicating broadband three-wave mixing processes.

We then measure the photon-pair generation from the type-I SPDC process in the 4H-SiC waveguide with a mode converter (Figure 1a). In the measurement setup (**Figure 3a**), the pump light at 775 nm from a visible CW laser is set to be the TE polarization through a polarization controller (PC), and is coupled into the device under test (DUT) through a lensed fiber. The ADC mode converter (Figure 1b) converts the SH mode from TE_{00} to

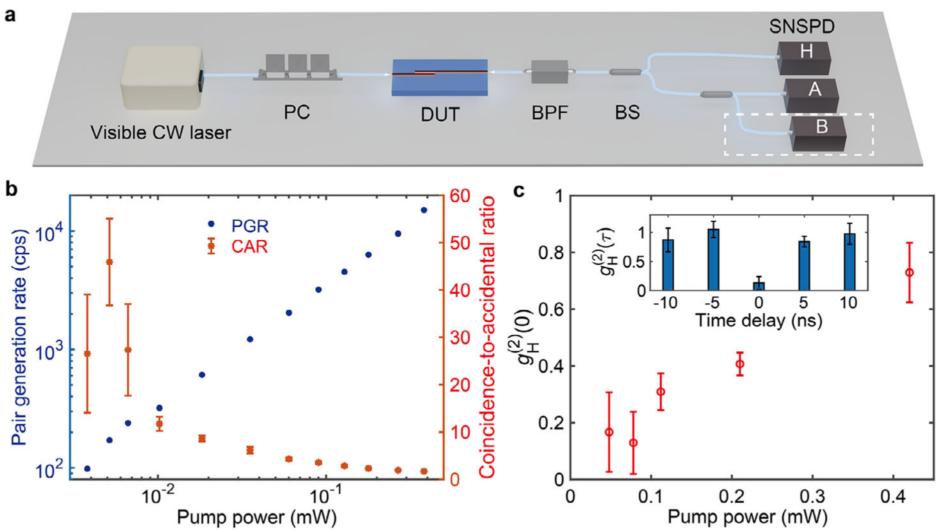

Figure 3. Photon-pair generation in 4H-SiC waveguide. a) Experimental setup. Visible CW laser: visible continuous-wave laser (775 nm); PC: polarization controller; DUT: device under test; BPF: bandpass filter; BS: beam splitter; SNSPD: superconducting nanowire single-photon detector. b) Photon-pair generation rate (PGR, blue) and coincidence-to-accidental ratio (CAR, red) versus on-chip pump power. c) Measured heralded second-order correlation at zero time delay ($g_H^{(2)}(0)$) as a function of on-chip pump power. Inset: measured heralded second-order correlation at different time delays ($g_H^{(2)}(\tau)$) with a pump power of 0.08 mW, and it is measured to be 0.13 at zero time delay, indicating the measurements are operated in the single-photon regime.

TM_{20} in the adjacent waveguide to meet the phase-matching condition of the nonlinear interaction with the FH TE_{00} mode. Telecom photon pairs generated in the waveguide are coupled out using another lensed fiber. A bandpass filter (1542.5 – 1575.5 nm) with an extinction ratio of 40 dB is used to select the telecom photon pairs, and at the same time to filter the pump residue and other noise photons. Signal and idler photons within the filter bandwidth are separated by a 50/50 beam splitter (BS) and sent to superconducting nanowire single-photon detectors (SNSPDs) for coincidence counting with detectors H and A (Figure 3a).

We measure the photon-pair generation rate from the device at different pump powers. Taking into account the detection loss in signal/idler path (14.4 dB), we calculate the on-chip pair-generation rate (PGR) and extract the coincidence-to-accidental ratio (CAR) as a function of the pump power (Figure 3b). The PGR scales linearly as pump power, with an efficiency of 3.4×10^4 Hz mW^{-1} within the selected 15 nm filter bandwidth. The CAR reaches a maximum of 46 at 0.2 μW on-chip pump power, and becomes lower at high power, which is likely limited by multi-photon generation, Raman scattering, and fluorescence.

The SPDC source can be used to produce heralded single photons. We test the photon-number purity by performing heralded second-order correlation measurements (Figure 3a). We send the signal photons into a heralding detector (H) and split the idler photons using a 50/50 BS and measure the coincidence as a function of time delay (τ) between the two detectors (A and B). The heralded second-order correlation is given by $g_H^{(2)}(\tau) = \frac{N_H N_{HAB}(\tau)}{N_{HA}(\tau) N_{HB}(\tau)}$, where N_H is the photon counts on detector H, $N_{HA/HB}$ is the coincidence counts between detector H and A/B, and N_{HAB} is the triple coincidence events among three detectors (H, A, and B).[46] Figure 3c shows the measured $g_H^{(2)}(0)$ as a function of the pump power. When the pump power is $\lesssim$0.2 mW, we get $g_H^{(2)}(0) < 0.5$, indicating that the measurements are in the single-photon regime. The inset shows $g_H^{(2)}(\tau)$ at a pump power of 0.08 mW, where a clear anti-bunching dip with $g_H^{(2)}(0) = 0.013$ is observed.

Besides the type-I second-order nonlinear processes, 4H-SiC also allows type-0 and type-II processes, which are triggered by d_{33} and d_{15}, respectively.[38] Type-0 SHG, where the incident fields and the generated fields all have the same polarization, is realized through MPM between the TM_{00} mode at 1550 nm and the TM_{20} mode at 775 nm. The width of the waveguide is designed to be ≈550 nm. The SHG and SFG results measured from the fabricated type-0 phase-matched single straight waveguide are shown in **Figure** 4a,b, respectively. The normalized SHG conversion efficiency is extracted to be 0.10 ± 0.01% $W^{-1}cm^{-2}$. Such low efficiency is probably due to mode instability. As the TM_{20} mode propagates through a waveguide with thickness variations, it can couple into another higher-order TM-polarized mode, resulting in reduced conversion efficiency. Because d_{33} in 4H-SiC is double of d_{31},[43] type-0 $\chi^{(2)}$ nonlinear processes are supposed to be more efficient than type-I processes, by controlling the SiC film thickness to better support the stable modal phase-matching conditions. Type-II SHG, where the FH fields have orthogonal polarizations, is realized through MPM among the TM_{00} and TE_{00} modes at 1550 nm and the TE_{20} mode at 775 nm. The width of the waveguide is designed to be ≈730 nm. The SHG and SFG results measured from the fabricated type-II phase-matched single straight waveguide are shown in Figure 4c,d, respectively. The normalized SHG conversion efficiency is extracted to be 1.5 ± 0.1% $W^{-1}cm^{-2}$. The phasematching function of the type-II nonlinear process is not spectrally symmetric, due to different dispersion of the two orthogonally polarized FH modes. Such phase matching is advantageous in many scenarios. For instance, type-II SPDC allows easy separation of the photon pairs in terms of polarization. It also allows more effective tailoring of the phase-matching function to produce photon pairs with high spectral

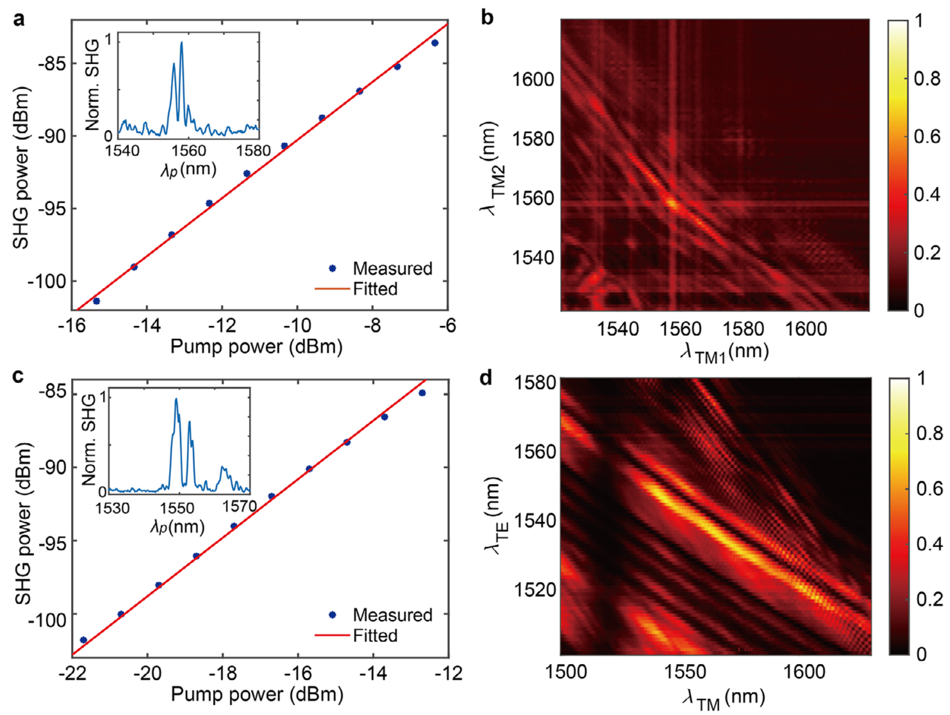

Figure 4. Type-0 and type-II phase-matched $\chi^{(2)}$ nonlinear interactions in 4H-SiC waveguides. a) Measured type-0 SHG power as a function of on-chip pump power at 1558 nm. A linear fitting reveals an on-chip conversion efficiency of $0.10 \pm 0.01\%$ $W^{-1}cm^{-2}$. Inset: normalized type-0 SHG spectrum. b) Measured type-0 SFG phase-matching function. c) Measured type-II SHG power as a function of on-chip pump power at 1549 nm. A linear fitting reveals an on-chip conversion efficiency of $1.5 \pm 0.1\%$ $W^{-1}cm^{-2}$. Inset: normalized type-II SHG spectrum. d) Measured type-II SFG phase-matching function.

Table 1. Three types of $\chi^{(2)}$ nonlinear interactions in 4H-SiC integrated platform demonstrated in this work.

Type	d	FH polarization	SH polarization	Waveguide width [nm]	η_{exp} [% W^{-1} cm^{-1}]
0	d_{33}	TM + TM	TM	550	0.1
I	d_{31}	TE + TE	TM	600	12.6
II	d_{15}	TE + TM	TE	730	1.5

purity.[47] Three types of $\chi^{(2)}$ nonlinear interactions in 4H-SiC integrated platform demonstrated in this work are summarized in **Table 1**.

3. Conclusion

In this work, we experimentally demonstrate various $\chi^{(2)}$ optical nonlinear processes on the 4H-SiCOI integrated photonic platform, with a particular focus on SPDC photon-pair generation. These results underscore the potential of 4H-SiC as a versatile material for nonlinear and quantum photonic applications. To further enhance the efficiency of $\chi^{(2)}$ nonlinear processes in this platform, improving the thickness uniformity of thin-film SiC is crucial, as it minimizes fluctuations in the optimal phase-matching wavelength along the waveguide. Additionally, employing a dual-layer SiC configuration with reverse polarities can enable MPM between the fundamental mode at the FH wavelength and the first-order mode at the SH wavelength, significantly improving nonlinear mode overlap. This approach has been shown to enhance SHG efficiency by one order of magnitude compared to conventional MPM methods used in this work.[48,49] Beyond material and structural optimizations, further advancements in fabrication and device design are essential to realize practical 4H-SiC quantum sources. Reducing waveguide propagation losses through improved etching techniques, enhancing source brightness via cavity integration, and increasing fiber-chip coupling efficiency with optimized mode-size converters will all contribute to higher heralding efficiency and improved overall performance. These improvements will pave the way for more efficient quantum photonic devices based on 4H-SiC. In addition, the ability to integrate SiC quantum light sources monolithically with other functional components represents a pivotal step towards scalable and practical on-chip quantum information processing systems. The potential for operating in harsh environments owing to SiC's stable physical properties and high chemical inertness will further make it a suitable material for next-generation quantum technologies in space applications.

Acknowledgements

This research is supported by the National Research Foundation Singapore (NRF2022-QEP2-01-P07, NRF-NRFF15-2023-0005), A*STAR (C230917005, M23M7c0125), and Villum Fonden (VIL50293).

Conflict of Interest

The authors declare no conflict of interest.

Data Availability Statement

The data that support the findings of this study are available from the corresponding author upon reasonable request.

Keywords

photon-pair generation, silicon carbide, spontaneous parametric down-conversion

Received: January 15, 2025
Revised: March 25, 2025
Published online:

[1] A. Elasser, T. P. Chow, *Proc. IEEE* **2002**, *90*, 969.
[2] H. Ou, Y. Ou, A. Argyraki, S. Schimmel, M. Kaiser, P. Wellmann, M. K. Linnarsson, V. Jokubavicius, J. Sun, R. Liljedahl, M. Syväjärvi, *Eur. Phys. J. B* **2014**, *87*, 1.
[3] S. Castelletto, A. Peruzzo, C. Bonato, B. C. Johnson, M. Radulaski, H. Ou, F. Kaiser, J. Wrachtrup, *ACS Photonics* **2022**, *9*, 1434.
[4] H. Ou, X. Shi, Y. Lu, M. Kollmuss, J. Steiner, V. Tabouret, M. Syväjärvi, P. Wellmann, D. Chaussende, *Materials* **2023**, *16*, 1014.
[5] X. Shi, J. Zhang, W. Fan, Y. Lu, N. Peng, K. Rottwitt, H. Ou, *Photonics Res.* **2022**, *10*, A8.
[6] A. Yi, C. Wang, L. Zhou, Y. Zhu, S. Zhang, T. You, J. Zhang, X. Ou, *Appl. Phys. Rev.* **2022**, *9*, 3.
[7] M. A. Guidry, K. Y. Yang, D. M. Lukin, A. Markosyan, J. Yang, M. M. Fejer, J. Vučković, *Optica* **2020**, *7*, 1139.
[8] A. A. Afridi, Y. Lu, X. Shi, R. Wang, J. Li, Q. Li, H. Ou, *Appl. Phys. Lett.* **2024**, *124*, 17.
[9] X. Shi, W. Fan, Y. Lu, A. K. Hansen, M. Chi, A. Yi, X. Ou, K. Rottwitt, H. Ou, *APL Photonics* **2021**, *6*, 7.
[10] X. Shi, W. Fan, A. K. Hansen, M. Chi, A. Yi, X. Ou, K. Rottwitt, H. Ou, *Advanced Photonics Res.* **2021**, *2*, 2100068.
[11] L. Cai, J. Li, R. Wang, Q. Li, *Photonics Res.* **2022**, *10*, 870.
[12] R. Wang, J. Li, L. Cai, Q. Li, *Opt. Lett.* **2023**, *48*, 1482.
[13] J. Li, R. Wang, A. A. Afridi, Y. Lu, X. Shi, W. Sun, H. Ou, Q. Li, *ACS photonics* **2024**, *11*, 795.
[14] C. Wang, J. Li, A. Yi, Z. Fang, L. Zhou, Z. Wang, R. Niu, Y. Chen, J. Zhang, Y. Cheng, J. Liu, C.-H. Dong, X. Ou, *Light: Sci. Appl.* **2022**, *11*, 341.
[15] F. Martini, A. Politi, *Appl. Phys. Lett.* **2018**, *112*, 25.
[16] J. Li, Q. Zhang, J. Wang, A. W. Poon, *Commun. Phys.* **2024**, *7*, 125.
[17] K. Powell, L. Li, A. Shams-Ansari, J. Wang, D. Meng, N. Sinclair, J. Deng, M. Lončar, X. Yi, *Nat. Commun.* **2022**, *13*, 1851.
[18] Y. Lu, X. Shi, A. Ali Afridi, Y. Wang, V. Tabouret, D. Chaussende, K. Rottwitt, H. Ou, *Opt. Lett.* **2024**, *49*, 4389.
[19] P. Xing, D. Ma, K. J. Ooi, J. W. Choi, A. M. Agarwal, D. Tan, *ACS Photonics* **2019**, *6*, 1162.
[20] Q. Zhang, J. Wang, A. W. Poon, *Photonics* **2024**, *11*, 8.
[21] X. Shi, Y. Lu, H. Ou, *Opt. Lett.* **2023**, *48*, 616.
[22] X. Shi, Y. Lu, N. Peng, K. Rottwitt, H. Ou, *J. Lightwave Technol.* **2022**, *40*, 7626.
[23] S. Pirandola, B. R. Bardhan, T. Gehring, C. Weedbrook, S. Lloyd, *Nat. Photonics* **2018**, *12*, 724.
[24] Y.-A. Chen, Q. Zhang, T.-Y. Chen, W.-Q. Cai, S.-K. Liao, J. Zhang, K. Chen, J. Yin, J.-G. Ren, Z. Chen, S.-L. Han, Q. Yu, K. Liang, F. Zhou, X. Yuan, M.-S. Zhao, T.-Y. Wang, X. Jiang, L. Zhang, W.-Y. Liu, Y. Li, Q. Shen, Y. Cao, C.-Y. Lu, R. Shu, J.-Y. Wang, L. Li, N.-L. Liu, F. Xu, X.-B. Wang, et al., *Nature* **2021**, *589*, 214.
[25] A. I. Lvovsky, B. C. Sanders, W. Tittel, *Nat. Photonics* **2009**, *3*, 706.
[26] S. Mukamel, M. Freyberger, W. Schleich, M. Bellini, A. Zavatta, G. Leuchs, C. Silberhorn, R. W. Boyd, L. L. Sánchez-Soto, A. Stefanov, M. Barbieri, A. Paterova, L. Krivitsky, S. Shwartz, K. Tamasaku, K. Dorfman, F. Schlawin, V. Sandoghdar, M. Raymer, A. Marcus, O. Varnavski, T. Goodson III, Z.-Y. Zhou, B.-S. Shi, S. Asban, M. Scully, G. Agarwal, T. Peng, A. V. Sokolov, Z.-D. Zhang, M. S. Zubairy, I. A. Vartanyants, E. del Valle, F. Laussy, *J. Phys. B: At., Mol. Opt. Phys.* **2020**, *53*, 072002.
[27] S. Castelletto, A. Boretti, *J. Phys. Photonics* **2020**, *2*, 022001.
[28] H. Ou, *Light: Sci. Appl.* **2024**, *13*, 219.
[29] R. Nagy, M. Niethammer, M. Widmann, Y.-C. Chen, P. Udvarhelyi, C. Bonato, J. U. Hassan, R. Karhu, I. G. Ivanov, N. T. Son, J. R. Maze, T. Ohshima, Ö. O. Soykal, Á. Gali, S.-Y. Lee, F. Kaiser, J. Wrachtrup, *Nat. Commun.* **2019**, *10*, 1.
[30] A. L. Crook, C. P. Anderson, K. C. Miao, A. Bourassa, H. Lee, S. L. Bayliss, D. O. Bracher, X. Zhang, H. Abe, T. Ohshima, E. L. Hu, D. D. Awschalom, *Nano Lett.* **2020**, *20*, 3427.
[31] S. Castelletto, B. Johnson, V. Ivády, N. Stavrias, T. Umeda, A. Gali, T. Ohshima, *Nat. Mater.* **2014**, *13*, 151.
[32] A. Lohrmann, N. Iwamoto, Z. Bodrog, S. Castelletto, T. Ohshima, T. Karle, A. Gali, S. Prawer, J. McCallum, B. Johnson, *Nat. Commun.* **2015**, *6*, 7783.
[33] J.-F. Wang, Z.-H. Liu, F.-F. Yan, Q. Li, X.-G. Yang, L. Guo, X. Zhou, W. Huang, J.-S. Xu, C.-F. Li, G.-C. Guo, *Acs Photonics* **2020**, *7*, 1611.
[34] L. Spindlberger, A. Csóré, G. Thiering, S. Putz, R. Karhu, J. U. Hassan, N. Son, T. Fromherz, A. Gali, M. Trupke, *Phys. Rev. Appl.* **2019**, *12*, 014015.
[35] B. Diler, S. J. Whiteley, C. P. Anderson, G. Wolfowicz, M. E. Wesson, E. S. Bielejec, F. Joseph Heremans, D. D. Awschalom, *npj Quantum Inf.* **2020**, *6*, 11.
[36] A. Rahmouni, R. Wang, J. Li, X. Tang, T. Gerrits, O. Slattery, Q. Li, L. Ma, *Light: Sci. Appl.* **2024**, *13*, 110.
[37] S. N. Rashkeev, W. R. Lambrecht, B. Segall, *Phys. Rev. B* **1998**, *57*, 9705.
[38] X. Shi, Y. Lu, S. Wang, V. Dhyani, S. S. Mohanraj, V. Leong, J. Zhang, H. Ou, D. Zhu, in *CLEO: Science and Innovations*, Optica Publishing Group, Washington, DC **2024**, p. SM4N–3.
[39] D. M. Lukin, C. Dory, M. A. Guidry, K. Y. Yang, S. D. Mishra, R. Trivedi, M. Radulaski, S. Sun, D. Vercruysse, G. H. Ahn, J. Vučković, *Nat. Photonics* **2020**, *14*, 330.
[40] D. Zhu, L. Shao, M. Yu, R. Cheng, B. Desiatov, C. Xin, Y. Hu, J. Holzgrafe, S. Ghosh, A. Shams-Ansari, E. Puma, N. Sinclair, C. Reimer, M. Zhang, M. Lončar, *Adv. Opt. Photonics* **2021**, *13*, 242.
[41] S. Signorini, L. Pavesi, *AVS Quantum Science* **2020**, *2*, 4.
[42] T. Pliska, D. Fluck, P. Günter, L. Beckers, C. Buchal, *J. Appl. Phys.* **1998**, *84*, 1186.
[43] H. Sato, M. Abe, I. Shoji, J. Suda, T. Kondo, *JOSA B* **2009**, *26*, 1892.
[44] H. Sato, I. Shoji, J. Suda, T. Kondo, in *Materials Science Forum*, vol. *615*, Trans Tech Publ, Switzerland **2009**, pp. 315-318.
[45] E. J. Stanton, J. Chiles, N. Nader, G. Moody, N. Volet, L. Chang, J. E. Bowers, S. Woo Nam, R. P. Mirin, *Opt. Express* **2020**, *28*, 9521.
[46] K. Guo, L. Yang, X. Shi, X. Liu, Y. Cao, J. Zhang, X. Wang, J. Yang, H. Ou, Y. Zhao, *Phys. Rev. Appl.* **2019**, *11*, 034007.
[47] C. Xin, J. Mishra, C. Chen, D. Zhu, A. Shams-Ansari, C. Langrock, N. Sinclair, F. N. Wong, M. Fejer, M. Lončar, *Opt. Lett.* **2022**, *47*, 2830.
[48] X. Shi, S. S. Mohanraj, V. Dhyani, A. A. Baiju, S. Wang, J. Sun, L. Zhou, A. Paterova, V. Leong, D. Zhu, *Light: Sci. Appl.* **2024**, *13*, 282.
[49] L. Wang, X. Zhang, F. Chen, *Laser Photonics Rev.* **2021**, *15*, 2100409.